



How to cite this article:

Badarul Azam, A. S., Jumaat, A. K., Badarul Azam, A. B., Mohammad Sabri, N. A. S., Yahaya, A. M., Ismail, A. T., Abdul Razak, M. A., Maasar, M. A., & Laham, M. F.(2024). Restoration and segmentation of Old Jawi Manuscripts using variational image inpainting and active contour models. *Journal of Information and Communication Technology*, 23(4), 561-592. <https://doi.org/10.32890/jict2024.23.4.1>

Restoration and Segmentation of Old Jawi Manuscripts using Variational Image Inpainting and Active Contour Models

¹Akmal Shafiq Badarul Azam, ²Abdul Kadir Jumaat

³Amisha Balkis Badarul Azam ⁴Nur Afiqah Sabirah

Mohammad Sabri, ⁵Amiratul Munirah Yahaya,

⁶Ahmad Thaqif Ismail, ⁷Muhammad Anas Abdul Razak,

⁸Mohd Azdi Maasar & ⁹Mohamed Faris Laham

¹School of Mathematical Sciences, College of Computing,
Informatics and Mathematics,

Universiti Teknologi MARA, Mukah, Malaysia

^{2,3&4}School of Mathematical Sciences,

College of Computing, Informatics and Mathematics, Universiti
Teknologi MARA, Shah Alam, Malaysia

^{5&6}Academy of Contemporary Islamic Studies,

Universiti Teknologi MARA, Shah Alam, Malaysia

⁷Arabic Language Department,

Academy of Language Studies,

Universiti Teknologi MARA, Mukah, Malaysia

⁸Mathematical Sciences Studies, College of Computing,
Informatics and Mathematics, Seremban Campus,

Universiti Teknologi MARA, Negeri Sembilan Malaysia

⁹Institute for Mathematical Research,

Universiti Putra Malaysia, Malaysia

²Institute for Big Data Analytics and Artificial Intelligence

Universiti Teknologi MARA, Shah Alam, Malaysia

¹akmalshafiq@uitm.edu.my
^{*2}abdulkadir@tmsk.uitm.edu.my
³2020834184@student.uitm.edu.my
⁴2020834632@student.uitm.edu.my
⁵amiratul@uitm.edu.my
⁶thaqif@uitm.edu.my
⁷anasrazak@uitm.edu.my
⁸azdimaasar@tmsk.uitm.edu.my
⁹mohdfaris@upm.edu.my
^{*}Corresponding author

Received: 17/3/2024 Revised: 3/9/2024 Accepted: 10/10/2024 Published: 28/10/2024

ABSTRACT

Old Jawi Manuscripts (OJM) are crucial to historical studies, offering insights into past societies. However, degradation from mishandling and environmental factors can impair their legibility. To preserve OJM, image inpainting and segmentation are essential for restoring corrupted areas and identifying text. Recently, the Gaussian Regularization Segmentation (GRS) model has shown effectiveness in intensity inhomogeneity grayscale image segmentation, though it was not designed for corrupted OJM images. Therefore, this study aimed to reformulate the GRS model to restore and segment text from real corrupted OJM images. The methodology begins with the incorporation of the Mumford-Shah and Bertalmio inpainting models into the GRS model as new fitting terms, resulting in the Modified Gaussian Regularization Segmentation Mumford-Shah (MGRSM) model and the Modified Gaussian Regularization Segmentation Bertalmio (MGRSB) model, respectively. MATLAB was used to implement these models, and their performance was assessed on 30 corrupted OJM samples from Malay Ethnomathematics Research Group, with expert evaluations and efficiency measured by average elapsed time. The MGRSM model achieved 38.4 percent and 12.4 percent higher overall total scores from experts in terms of segmentation accuracy compared to the GRS and MGRSB models, respectively. While the GRS model is the fastest, the MGRSM model provides superior accuracy, with an average processing time of 9.35 seconds, making it the most optimal for restoring and segmenting OJM images. This approach not only enhances the preservation of

historical manuscripts but also provides a practical tool for researchers and historians in safeguarding our cultural heritage.

Keywords: Active contour, historical document, image segmentation, image inpainting, old Jawi manuscript.

INTRODUCTION

In the Malay realm, Jawi has persisted for millennia as a form of writing, deeply rooted in the region's history and intimately tied to the arrival of Islam. Jawi is a script that utilizes Arabic letters to write Malay and several other Malay-speaking languages (Razak, 2016; Zainal et al., 2022). Within museums, libraries, and archives, old Jawi manuscripts (OJM) are preserved as significant artifacts of national heritage, containing invaluable insights into the culture and values of historical communities. However, these manuscripts face unique challenges in preservation, particularly in image segmentation and restoration.

OJM are often affected by various forms of degradation, including light exposure, which can permanently fade their colors, and environmental factors such as heat, moisture, and microbial growth, all of which can lead to text obscurity (Ventzas et al., 2012; Kaur et al., 2020). Unlike other historical documents, Jawi manuscripts present additional difficulties due to the script's complexity in combining Arabic characters with unique diacritics specific to Malay, complicating the segmentation process. Furthermore, the degradation in OJMs tends to be non-uniform, with localized damages like scratches and ink smudging, making restoration particularly challenging (Razak, 2016). Therefore, specialized image inpainting and segmentation techniques are crucial to effectively preserve these precious manuscripts.

Image inpainting is the process of completing incomplete visual input details. The primary objective is to reconstruct missing portions or cracked images so that a casual observer cannot trace the inpainted area (Zainal et al., 2022). Recently, image inpainting models have been used to remove distracting objects from an image (Yu et al., 2019), restore corrupted ancient painting images (Jaidilert & Farooque, 2018), and fill up degraded images in ancient Indian manuscripts (Kaur et al., 2020). While learning-based approaches by Zhao et al. (2019) and Zhang et al. (2020) have shown promising

results, they often rely heavily on large datasets. Additionally, user-guided methods, such as boundary lines, extended directions, guide regions, and image exemplars, have been explored by Ashikhmin (2001), Hays and Efros (2023), Huang et al. (2013), and Yu et al. (2019), but these approaches tend to be structured and lack flexibility for content-based adaptability.

Zainal et al. (2022) applied two effective and well-known inpainting models, namely the Mumford and Shah (1989) and Bertalmio (2001) inpainting models, to restore OJM. They compared the Mumford and Bertalmio inpainting models using artificially corrupted OJM images rather than real corrupted OJM images and deliberately introduced corruption into the OJM images before applying the image restoration process. Figure 1 illustrates the example of how the clean OJM image was transformed into its artificially corrupted form with a mask.

Figure 1

Example of Clean OJM Image, Mask and Corrupted OJM Image Using Mask

(a) Clean OJM Image	(b) Mask	(c) Corrupted OJM Image Using Mask

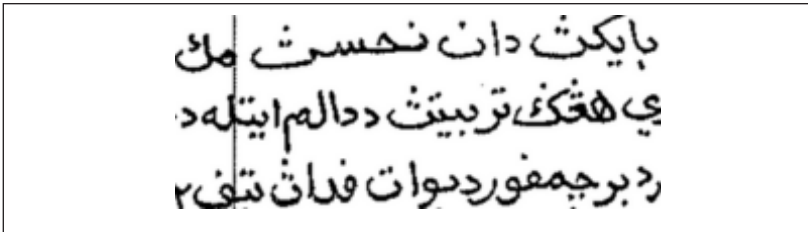
As shown in Figure 1(a), the process began with a clean OJM image, which served as the uncorrupted reference. The image was obtained from Malay Ethnomathematics Research Group (*Kumpulan Penyelidikan Etnomatematik Melayu*, 2021). A mask shown in Figure 1(b) was then applied to simulate corruption by covering specific areas of the clean OJM image. This masking introduced controlled imperfections, allowing the researchers to create a corrupted OJM image, as illustrated in Figure 1(c).

The advantage of using the procedure was that the researchers could compute quantitative metrics such as accuracy, precision, recall, or F1 score due to the availability of the ground truth image, which was the clean OJM image in Figure 1(a). To compute the quantitative metrics of the restoration models' performance, Zainal et al. (2022)

compared the OJM restoration outputs produced by the Mumford and Bertalmio inpainting models with the original clean OJM images. However, models tested on artificially corrupted images may perform differently when faced with genuine corruption. Figure 2 shows an example of a real corrupted OJM image obtained from the *Kumpulan Penyelidikan Etnomatematik Melayu* (2021) database.

Figure 2

An Example of Real Corrupted OJM Image



The image in Figure 2 is an example of an OJM image that had already been corrupted by vertical scratches on the left. In this study, the Mumford-Shah and Bertalmio image inpainting models were employed to restore the real corrupted OJM images. The Mumford-Shah inpainting model maintains smoothness while preserving sharp edges, making it ideal for image restoration. Its robust mathematical framework and efficient approximations, like the Ambrosio-Tortorelli method, allow for rapid and precise inpainting, even in images with intricate details (Zainal et al., 2022). Meanwhile, the Bertalmio inpainting model excels at reconstructing damaged or missing regions by using anisotropic diffusion, which effectively propagates surrounding information while preserving the natural structure and boundaries of the image (Barbu, 2018).

Image segmentation is one of the most intricate and crucial challenges in image processing. It involves dividing an image into multiple components (Azam et al., 2023). This task has become essential to a wide range of image-processing applications, including shape boundary recognition (Othman et al., 2016), medical imaging (Burrows et al., 2024; Mohd Sharif et al., 2024), and machine learning (Yousef et al., 2023). As in text recognition applications, image segmentation is required to binarize the input image and separate the text from the background. One of the successful image segmentation

models is the variational active contour model (ACM). The variational ACM minimizes the energy functional using variational calculus. It effectively drives the motion of contour curves towards the boundaries of desired objects and generates satisfying segmentation results for images with intensity features of varying intensities. This study utilized ACM due to its flexibility and adaptability. These models can dynamically adjust contours, handle complex boundaries, and easily integrate customized constraints and priors into the energy functionals, all within clear and understandable mathematical formulations (Gui et al., 2023).

ACM can be divided into two categories, which are the region-based and edge-based approaches (Ali et al., 2018). In this research, we focused on active contour region-based approaches as these methods outperform the edges-based approach for images with noise and fuzzy boundaries (Weng et al., 2021). The Chan-Vese model, created by Chan and Vese (2001), is one of the prominent region-based active contour models. This piecewise constant model extends the Mumford-Shah model that Mumford and Shah (1989) developed to a simple numerical representation without approximation. However, this model struggles with images with varying intensity levels, resulting in limited segmentation performance. To overcome this limitation, piecewise smooth models have been proposed, but they are often slow due to their complex procedures (Tsai et al., 2001; Vese & Chan, 2002).

The Local Image Fitting (LIF) model, introduced by Zhang et al. (2010), has gained significant traction in the field. This model effectively addresses the challenges posed by images with varying intensity levels and enhances segmentation speed. The LIF model achieves this by analyzing the differences between the original grayscale image and a locally fitted version. Additionally, the integration of a Gaussian function for variational level set regularization further boosts processing efficiency. The widespread adoption of the LIF model and Gaussian function among researchers is a testament to their effectiveness in segmenting images with varying intensity levels (Biswas & Hazra, 2021; Fang et al., 2021; Iqbal et al., 2020; Soomro et al., 2019; Yang et al., 2020). However, all these ACM models can produce over-segmented results when the region of interest (foreground) has intensities nearly identical to those of the background and when the contours are indistinct (Badshah et al., 2020).

To address the above problem, Saibin and Jumaat (2023) introduced the Gaussian Regularization Segmentation (GRS) model, an active contour region-based approach for segmenting regions of interest in grayscale images. They integrated local image-fitting energy and a distance function into the energy minimization process and applied a Gaussian function to regularize the level set function. This combination enables the GRS model to effectively handle images with varying intensity levels at low computational complexity, even when the targeted objects are close to neighboring regions. However, the GRS model may not perform optimally on OJM images compared to general image types due to their unique characteristics, such as intricate script, non-uniform degradation, and localized damage, such as scratches. Numerous segmentation models have been utilized in the literature on OJM to separate the text from the background. These include the thresholding method (Baihaqi et al., 2024; Devadass et al., 2021; Ismail & Abdullah, 2014; Mahmor et al., 2018; Saddami et al., 2017; Som et al., 2011; Yahya et al., 2018; Zulcaffle et al., 2010) and the combination of vertical histogram projection and sliding window technique (Razak, 2016). To the best of our knowledge, no researcher had applied a variational active contour model to segment the text of the OJM images from its background.

Motivated by this, we proposed modified active contour region-based models to effectively restore and segment the text (foreground) in real corrupted OJM images. This can be accomplished by reformulating the GRS model, where the information from the image inpainting techniques, namely the Mumford-Shah and Bertalmio inpainting models, were substituted in the fitting term of the GRS model. By modifying the GRS model, image quality and segmentation accuracy were anticipated to improve. The upcoming section outlines the related works and research methodology used to reformulate the proposed models. Following that, the experimental results of both the existing and proposed models were discussed.

RELATED WORKS

This section reviews the existing literature on segmentation techniques for OJM images, focusing on various approaches and their effectiveness. It highlights the strengths and limitations of these methods, providing a context for the proposed modifications to the GRS model. Table 1 summarizes key research studies that focused on segmentation methods for OJM.

Table 1
Summary of Recent Previous Works on OJM Segmentation

Author (Year)	Segmentation Method	Strength	Limitation
Zulcaifle et al. (2010)	Novel thresholding algorithm with morphological operations and iterative techniques	Superior performance against noise; enhances text clarity	Ineffective for handling corrupted parts as no image inpainting technique was used
Som et al. (2011)	Thresholding methods: Otsu (global), Niblack, and Sauvola (local)	Local thresholding enhances readability, particularly Niblack	The technique segments the Jawi text as well as the image noise
Ismail and Abdullah (2014)	Combination of Global enhancement and local adaptive thresholding	Outperforms established methods; enhances readability	Struggles with noisy images; ineffective for handling corrupted part
Razak (2016)	Vertical histogram projection and sliding window technique	High segmentation accuracy; innovative approach	Segments image noise/corrupted parts along with the target regions (Jawi text)
Saddami et al. (2017)	Improved thresholding: Dynamic boundary calculation based on standard deviation	Effective in-text segmentation; reduces false foreground pixels	Potential introduction of noise in empty areas; segments noise/corrupted parts along with the target regions (Jawi text)
Yahya et al. (2018)	Adaptive Threshold Filtering Process (PAM)	Higher precision rate; effective text enhancement	Does not incorporate image inpainting techniques to restore corrupted areas
Mahmor et al. (2018)	Global thresholding methods: Huang, Kapur, Otsu and Yen	Yen method provides the best results for distinguishing foreground and background	Performance may vary based on image characteristics; some methods less effective in low contrast situations; Ineffective for handling corrupted part as no image inpainting technique was used
Devadass et al. (2021)	Combination of thresholding and local image enhancement method	Simple and fast computation segmentation	Ineffective for handling corrupted part as no image inpainting technique was used
Baihaqi et al. (2024)	Combination of thresholding method with histogram equalization method	The use of histogram equalization method improves image quality by eliminating foxing and improving the contrast between text and background	Segments image noise/corrupted parts along with the target regions (Jawi text)

Based on Table 1, thresholding is the most commonly used method for segmenting Jawi text (foreground) from the background. Som et al. (2011) evaluated various thresholding techniques, including the Otsu global method and local methods by Niblack and Sauvola. Their experimental results showed that local methods, particularly Niblack, outperformed global methods in terms of readability, character recognition, and computational efficiency. However, the technique segments the Jawi text as well as the image noise.

In addition to the findings of Som et al. (2011), Mahmor et al. (2018) explored global thresholding methods, including Huang, Kapur, Otsu, and Yen, specifically for the Terengganu Inscribed Stone. Their study concluded that the Yen method yielded the best results for distinguishing foreground from background in Jawi manuscripts. However, they also noted that the effectiveness of these methods could vary depending on image characteristics, particularly in low-contrast situations.

To improve segmentation accuracy, many researchers have focused on refining thresholding techniques. For example, Zulcaffle et al. (2010) introduced a novel algorithm that combines morphological operations with iterative thresholding techniques, outperforming traditional methods like Niblack and Sauvola, as validated by visual inspection and quantitative metrics. A key strength of this approach is its resilience to various types of noise in degraded OJM, significantly enhancing text clarity. Additionally, Saddami et al. (2017) proposed an improved thresholding method for segmentation, enhancing the NICK (an improved version of Niblack) method by dynamically calculating boundary values for objects within window values based on the image's standard deviation. This method is particularly effective in segmenting text, especially in extracting thin strokes and reducing false foreground pixels. However, its limitation lies in the potential introduction of noise in empty areas of the OJM images, which may affect the overall quality of the segmentation results.

On the other hand, many researchers have combined thresholding methods with image enhancement techniques (Devadass et al., 2021; Ismail & Abdullah, 2014; Yahya et al., 2018). Recently, Baihaqi et al. (2024) integrated thresholding with histogram equalization to enhance text visibility in corrupted OJM. Histogram equalization improves image quality by reducing foxing and increasing contrast

between the text and background. Aside from the thresholding method, Razak (2016) introduced a novel segmentation method that combines vertical histogram projection with a sliding window technique. This approach effectively segments characters in manuscripts by detecting the spaces between characters and determining the maximum line height for accurate segmentation.

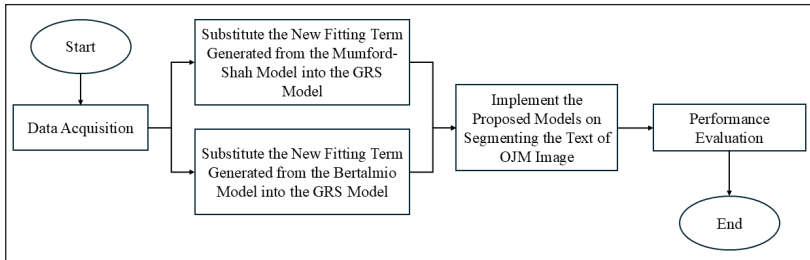
Despite the strengths of all the image segmentation methods mentioned above, they share a standard limitation: the absence of image inpainting techniques. Image inpainting is designed to restore corrupted areas in images. Without this technique, the segmentation methods also tend to segment the image noise that makes up the corrupted areas, leading to potential inaccuracies in segmenting both the corrupted regions and the target areas of Jawi text. Motivated by the significant limitations of existing models in restoring and segmenting text in real corrupted OJM images, we proposed modified active contour region-based models. By reformulating the GRS model to incorporate information from image inpainting techniques, specifically the Mumford-Shah and Bertalmio models, we aimed to address these shortcomings. This integration is anticipated to enhance both image quality and segmentation accuracy, making it a crucial advancement in the field of image processing and computer vision.

METHODOLOGY

In this section, the research methodology for our proposed models was discussed. Figure 3 shows the flow of the methodology involved in this study.

Figure 3

Research Methodology Framework



As shown in Figure 3, the initial step involved obtaining a set of 30 real corrupted OJM images from *Kumpulan Penyelidikan Etnomatematik Melayu* (2021). Subsequently, the procedure involved acquiring the new fitting terms of an input OJM image generated by the Mumford-Shah and Bertalmio inpainting models. These new fitting terms were substituted into the energy minimization functional of the GRS model to segment the text of OJM images. Finally, the segmentation results obtained were evaluated to assess the performance of the proposed models. The following sub-section goes over each of these processes in depth.

Data Acquisition

This research involved the segmentation of 30 real corrupted images of OJM that were obtained from *Kumpulan Penyelidikan Etnomatematik Melayu* (2021). The OJM images were cropped and resized to the size of 24196 pixels. We remarked that all 30 cropped OJM images were originally corrupted by scratches, as indicated in Figure 2.

Mumford-Shah Inpainting Model

The Mumford-Shah inpainting model is defined in Equation 1:

$$\min_{v_M, \Gamma} \{E^M(v_M, \Gamma)\},$$

$$E^M(v_M, \Gamma) = \frac{\gamma}{2} \int_{\Omega \setminus \Gamma} |\nabla v_M|^2 dx + \alpha |\Gamma| + \frac{\lambda}{2} \int_{\Omega \setminus \Gamma} (v_M - v)^2 dx \quad (1)$$

where $\gamma > 0$, $\alpha > 0$ and $\lambda > 0$ are the weights of the terms. This model provided two outputs, which were an inpainted image v_M and its correlated edge image Γ from the input image v . The initial two terms assure a smooth output, whereas the last term prevents an overly smoothing effect. Meanwhile, $|\nabla v_M|$ denotes the norm of the gradient of the inpainted image and $|\Gamma|$ denotes the Euclidean length term. The model was effectively solved by an elliptic solver and iteration scheme. Details of the algorithm can be found in Tsai et al. (2001), Esedoglu and Shen (2002), Shen and Chan (2002) and Schönlieb (2015a). The algorithm was implemented in the MATLAB R2021a software.

Bertalmio Inpainting Model

The Bertalmio inpainting model is defined as Equation 2:

$$v_t = \nabla^\perp v_b \cdot \nabla \Delta v_b + v_q \nabla \cdot (g(|\nabla v_b|) \nabla v_b). \quad (2)$$

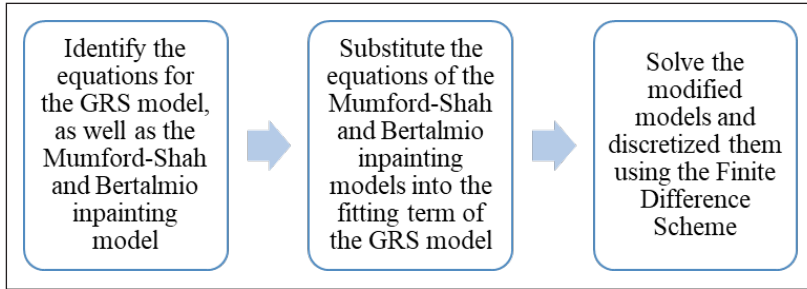
The first term was the transport equation, which was utilized to provide a smooth solution, and the second term was the anisotropic diffusion equation, which prevented level lines from crossing with a small weight parameter $\nu_q > 0$. The model was solved iteratively using the finite difference scheme. Details of the algorithm are discussed in Bertalmio (2001) and Schönlieb (2015b). The MATLAB R2021a software was used to implement this model.

Formulation of the Proposed Models

In this sub-section, we briefly explained how we reformulated the existing GRS model introduced by Saibin and Jumaat (2023). Generally, the GRS model was reformulated according to the following steps shown in Figure 4 as follows:

Figure 4

Steps to Reformulate the GRS Model with Image Inpainting Models



Assume that a marker set $C = \{w_\ell = (x_\ell^*, y_\ell^*) \in \Omega, 1 \leq \ell \leq n_\ell\} \subset \Omega$ with $n_1 \geq 3$ marker points will be placed near the boundary of a targeted object in a given image $v(x, y)$. This marker set C is used to initialize the level set function. Thus, the energy E^{GRS} minimization functional for the GRS model is defined in Equation 3:

$$\min_{\phi} \{E^{GRS}(\phi)\},$$

$$E^{GRS}(\phi) = \frac{1}{2} \int_{\Omega} \left(v - (r_1 H(\phi) + r_2 (1 - H(\phi))) \right)^2 d\Omega + \theta \int_{\Omega} H(\phi) F_d d\Omega. \quad (3)$$

Initially, the fitting term $\left(v - (r_1 H(\phi) + r_2 (1 - H(\phi))) \right)^2$ of the GRS model in Equation 3 is substituted with the information from two image inpainting techniques, namely the Mumford-Shah model (Equation 1)

and Bertalmio model (Equation 2). By rewriting Equations 1 and 2, the image inpainting models are now described as follows:

a) Mumford-Shah model as represented by Equation 4:

$$v_{MS} = \min_{v_M, \Gamma} \{E^M(v_M, \Gamma)\} \tag{4}$$

b) Bertalmio model as represented by Equation 5:

$$v_B = v_t = \nabla^\perp v_b \cdot \nabla \Delta v_b + v_q \nabla \cdot (g(|\nabla v_b|) \nabla v_b). \tag{5}$$

This study proposed two modified GRS models concerning two different image inpainting models based on Equation 4 and Equation 5. In this study, we named the two modified GRS models the Modified Gaussian Regularization Segmentation Mumford-Shah (MGRSM) model and the Modified Gaussian Regularization Segmentation Bertalmio (MGRSB) model.

Upon substitution of Equation 4, which was generated from the Mumford-Shah model, into the GRS model of Equation 3, we obtained the first modified model that is the MGRSM model, represented by Equation 6:

$$\begin{aligned} &\min_{\phi} \{E^{MGRSM}(\phi, r_{M1}, r_{M2})\}, \tag{6} \\ &E^{MGRSM}(\phi, r_{M1}, r_{M2}) = \frac{1}{2} \int_{\Omega} (v_{MS} - (r_{M1}H(\phi) + r_{M2}(1-H(\phi))))^2 \end{aligned}$$

Similarly, the combination of Equation 5, which was generated from the Bertalmio model with the GRS model of Equation 3, resulted in our second modified model that is the MGRSB model defined in Equation 7:

$$\begin{aligned} &\min_{\phi} \{E^{MGRSB}(\phi, r_{B1}, r_{B2})\}, \tag{7} \\ &E^{MGRSB}(\phi, r_{B1}, r_{B2}) = \frac{1}{2} \int_{\Omega} (v_B - (r_{B1}H(\phi) + r_{B2}(1-H(\phi))))^2 \\ &\quad + \theta \int_{\Omega} H(\phi) F_d d\Omega \end{aligned}$$

Denoted here, $\theta > 0$ is the weightage of the final term of Equations 6 and 7. The interior intensity averages are represented by r_{M1} and r_{B1} while the exterior intensity averages are represented by r_{M2} and r_{B2} in a local region that are used to address intensity inhomogeneity, which can be expressed in the following Equations 8, 9, and 10:

$$\begin{aligned} r_{M1}(x, y) &= k_{\sigma} * [H(\phi)v_{MS}] / k_{\sigma} * H(\phi) \\ r_{M2}(x, y) &= k_{\sigma} * [(1-H(\phi))v_{MS}] / k_{\sigma} * (1-H(\phi)) \end{aligned} \quad (8)$$

And

$$\begin{aligned} r_{B1}(x, y) &= k_{\sigma} * [H(\phi)v_B] / k_{\sigma} * [H(\phi)] \\ r_{B2}(x, y) &= k_{\sigma} * [(1-H(\phi))v_B] / k_{\sigma} * (1-H(\phi)). \end{aligned} \quad (9)$$

The function k_{σ} is a Gaussian kernel with standard deviation σ such that:

$$k_{\sigma} = e^{-\frac{(x^2+y^2)}{2\sigma^2}} \quad (10)$$

where the standard deviation σ can be presumed as a scale parameter that influences the region scalability from a small neighborhood to the entire image domain (Saibin & Jumaat, 2023).

By variational calculus, the affiliated Euler-Lagrange (EL) equation for Equation 6 and Equation 7 are defined in Equations 11 and 12, respectively:

$$-\delta(\phi) \left[(v_{MS} - r_{M1}H(\phi) - r_{M2}(1-H(\phi)))(r_{M1} - r_{M2}) - \theta F_d \right] = 0 \quad (11)$$

and

$$-\delta(\phi) \left[(v_B - r_{B1}H(\phi) - r_{B2}(1-H(\phi)))(r_{B1} - r_{B2}) - \theta F_d \right] = 0 \quad (12)$$

where the gradient descent flow of Equation 11 and Equation 12 can be obtained by applying the gradient descent method in Equations 13 and 14 as follows:

$$\frac{\partial \phi}{\partial t} = \delta(\phi) \left[(v_{MS} - r_{M1}H(\phi) - r_{M2}(1-H(\phi)))(r_{M1} - r_{M2}) - \theta F_d \right] \quad (13)$$

and

$$\frac{\partial \phi}{\partial t} = \delta(\phi) \left[(v_B - r_{B1}H(\phi) - r_{B2}(1-H(\phi)))(r_{B1} - r_{B2}) - \theta F_d \right] \quad (14)$$

where $\frac{\partial \phi}{\partial t}$ is denoted as the evolution of ϕ with respect to artificial time t . To discretize Equation 13 and Equation 14, a forward finite difference scheme was employed, yielding the following Equations 15 - 18:

$$\frac{\phi_{i,j}^{k+1} - \phi_{i,j}^k}{\Delta t} = \delta(\phi_{i,j}^k) \left[(v_{MS} - r_{M1}H(\phi^k) - r_{M2}(1-H(\phi^k)))(r_{M1} - r_{M2}) - \theta F_d \right] \quad (15)$$

and

$$\frac{\phi_{i,j}^{k+1} - \phi_{i,j}^k}{\Delta t} = \delta(\phi_{i,j}^k) \left[(v_B - r_{B1}H(\phi^k) - r_{B2}(1-H(\phi^k)))(r_{B1} - r_{B2}) - \theta F_d \right]. \quad (16)$$

Lastly, we obtained $\phi_{i,j}^{k+1}$ by rearranging the above equation as follows:

$$\phi_{i,j}^{k+1} = \phi_{i,j}^k + \Delta t \delta(\phi_{i,j}^k) \left[(v_{MS} - r_{M1}H(\phi^k) - r_{M2}(1-H(\phi^k)))(r_{M1} - r_{M2}) - \theta F_d \right] \quad (17)$$

and

$$\phi_{i,j}^{k+1} = \phi_{i,j}^k + \Delta t \delta(\phi_{i,j}^k) \left[(v_B - r_{B1}H(\phi^k) - r_{B2}(1-H(\phi^k)))(r_{B1} - r_{B2}) - \theta F_d \right]. \quad (18)$$

where Δt is denoted as timestep. To ensure the regularity of the level set function ϕ and enhance the efficiency of contour evolution, the Gaussian function was convolved with the level set function. The resulting output at each iteration served as the initial condition for the subsequent iteration. This cycle was repeated for each iteration until the stopping criteria were met, which was either $\|\phi^{k+1} - \phi^k\| / \|\phi^k\| \leq tol$ or maximum iteration reaching 3000 iterations where tol was the prescribed tolerance value.

Algorithms to Implement the Proposed Models

In this study, the MATLAB R2021a software with an AMD Ryzen 5 3500U with Radeon Vega Mobile Gfx CPU running at 2.10 GHz and equipped with 4GB of RAM was utilized to implement the proposed models. The computational complexity was approximately $O(k^2 \times N)$ due to solving via the gradient descent method where N is the image size with iteration number, k (Zhang et al., 2010). Algorithm 1 shows the steps associated with the implementation process for the MGRSM model.

Algorithm 1: Algorithm to implement the MGRSM model

- 1) Set the value of parameters and define a set of initial markers C based on the size of the OJM image.
 - 2) Initialize the level set function ϕ such that Γ is the boundary of the initial polygon G construct from the marker set C .
-

(continued)

Algorithm 1: Algorithm to implement the MGRSM model

- 3) **For** $iteration = 1$ to $maxit$ or $\frac{\|\phi^{k+1} - \phi^k\|}{\|\phi^k\|} \leq tol$ **do**
- Compute $r_{M1}(\phi^k)$ and $r_{M2}(\phi^k)$ using Equation 8.
 Solve the level set function ϕ based on Equation 17.
 Regularize ϕ by convolving with k_σ .
- end for**
- The output ϕ is defined as the final solution.
-

Next, we discuss Algorithm 2 for the MGRSB model. All steps in the MGRSB model were identical to the algorithm in the MGRSM model except for step 3, where the local inner and intensity averages were computed using Equation 9 and the level set function ϕ evolved based on Equation 18.

Algorithm 2: Algorithm to implement the MGRSB model

- 1) Set the value of parameters and define initial set markers C based on the size of the OJM image.
- 2) Initialize the level set function ϕ such that Γ is the boundary of the initial polygon G construct from the marker set C .
- 3) **For** $iteration = 1$ to $maxit$ or $\frac{\|\phi^{k+1} - \phi^k\|}{\|\phi^k\|} \leq tol$ **do**
- Compute $r_{M1}(\phi^k)$ and $r_{M2}(\phi^k)$ using Equation 9.
 Solve the level set function ϕ based on Equation 18.
 Regularize ϕ by convolving with k_σ .
- end for**
- 4)The output ϕ is defined as the final solution.
-

Performance Evaluation

In this research, we assessed the performance of our proposed models in terms of segmentation accuracy and efficiency results. Since we utilized the original corrupted OJM images in our research, there were no ground truth OJM images available. As a result, it was not possible to use quantitative metrics such as accuracy, precision, recall, or F1 score. Therefore, we relied on expert evaluation and qualitative measures for assessing segmentation accuracy. Initially, two experts from the Academy of Contemporary Islamic Studies (ACIS) and an expert from the Academy of Language Studies at Universiti Teknologi MARA (UiTM) were selected. These experts were then instructed to assess each segmentation output image using a Likert scale ranging

from the following scale: 1 (Very Bad), 2 (Bad), 3 (Neutral), 4 (Good) and 5 (Very Good). The percentage of the total overall scores given by the experts was calculated to evaluate the segmentation performance.

Furthermore, this research also evaluated the efficiency of the proposed models by analyzing the elapsed time processing. Accurate measurement of elapsed time processing was attained using the ‘tic’ and ‘toc’ functions in the MATLAB R2021a software. To ensure reliable outcomes, the experiment was repeated three times, and the average elapsed time processing was calculated using Equation 19 as follows:

$$\text{Average Elapsed Time Processing, } \bar{t} = \frac{1}{3} \sum_{j=1}^3 t_j \quad (19)$$

where $\sum_{j=1}^3 t_j$ represents the sum of three readings of elapsed time processing.

RESULTS AND DISCUSSION

Two experiments were carried out. Firstly, we compared the accuracy and efficiency of the segmentation results of 30 real corrupted OJM images obtained from the GRS model developed by Saibin and Jumaat (2023), along with our two proposed MGRSM and MGRSB models. Following the outcomes of the first experiment, we opt for the more effective segmentation model between the MGRSM and MGRSB models to conduct parameter sensitivity analysis.

For the parameter settings, we maintained a fixed value of epsilon $\varepsilon = 1$, tolerance $tol = 0.005$, timestep $\Delta t = 0.001$, theta $\theta = 5000$, maximum iteration $iter = 3000$ and standard deviation $\varsigma = 0.45$ parameters for all models. However, the specific values of the standard deviation σ parameter varied between 10 and 50 for each model, depending on the individual OJM images.

Experiment 1: Segmentation Results on Real Corrupted OJM Images

As explained in the previous section, the MGRSM and MGRSB models proposed in this study were newly modified active contour region-based models. These models incorporate information from

image inpainting techniques, specifically the Mumford-Shah and Bertalmio inpainting models, respectively, into the fitting term of the GRS model. To assess the effectiveness of our proposed models in segmenting text on real corrupted OJM images, we compared our MGRSM and MGRSB models against the GRS model on a dataset consisting of 30 real corrupted OJM images. To determine the optimal model, we aggregated the total scores from all the experts for each segmented OJM image by GRS, MGRSM and MGRSB models and recorded the average elapsed time \bar{t} , as shown in Table 2 as follows.

Table 2

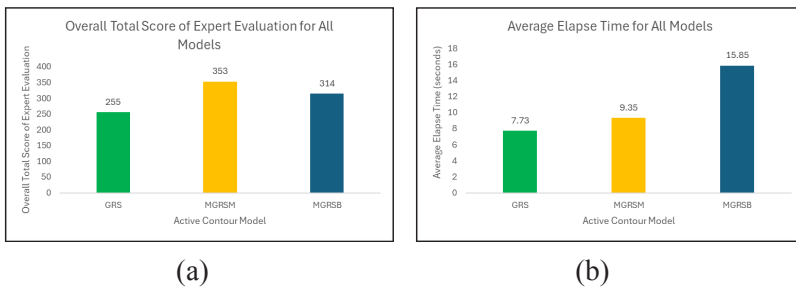
Overall Total Scores of Expert Evaluations and Average Elapse Time \bar{t}

Model	Expert 1 Total Scores	Expert 2 Total Scores	Expert 3 Total Scores	Overall Total Scores	\bar{t}
GRS	118	70	67	255	7.73
MGRSM	138	112	103	353	9.35
MGRSB	125	96	93	314	15.85

For better visual illustration purposes, we demonstrate the overall total score and the average elapsed time using a bar chart as shown in the following Figure 5.

Figure 5

Bar Chart for the Overall Total Score of Experts Evaluation and the Average Elapsed Time



As shown in Table 2 and Figure 5(a), the overall total score for the MGRSM model was the highest, with 353 overall total scores,

followed by the MGRSB and GRS models, with 314 and 255 overall total scores, respectively. This shows that the MGRSM was approximately 38.4 percent and 12.4 percent more accurate than the GRS and MGRSB models, respectively. Based on Figure 5(b), the average elapsed time t for the GRS model was the fastest, with 7.73 seconds, followed by the MGRSM model and the MGRSB model, with 9.35 and 15.85 seconds, respectively. It was understood that the slightly longer processing for the MGRSM and MGRSB models was primarily due to the incorporation of new fitting terms generated by the Mumford-Shah and Bertalmio inpainting models, respectively, in the mathematical formulation.

We chose six (out of 30) samples of real corrupted OJM images to illustrate the segmentation result by the GRS, MGRSM and MGRSB models. Figure 6 illustrates the chosen six real corrupted OJM images (Image 4, Image 10, Image 12, Image 26, Image 27 and Image 30).

Figure 6

Six Samples of the Real Corrupted OJM Images

 <p>بايکت دان نحسست مک بي هتکي تربيتت دالم ايتله د رد برجه غور ديوات فدات توف ۲</p>	 <p>لاکي ۲ پتخ کو بیخ کولیتن بر فاروت انوتاد زف دان سبایک ۲ هاری مولات برینیا بولوت در فزبتینا دان مکاشف یخ هاند</p>
<p>(a) Image 4</p>	<p>(b) Image 10</p>
 <p>بن فدوقت این بایک باغ اف فکرجان فون دبری ان مکرا فون فدوقت این بایک باغ اف فکرجان جمعه مالم تمت شهدان هارکین تلارن ایت مالک</p>	 <p>ابارغ مقصود کینت کتینای الله تعالی اخیرت عاری کتبت ایت مالک امیر جم فو کله یغاف یغاد کحاکن ایت سجا ی دری الله سجا</p>
<p>(c) Image 12</p>	<p>(d) Image 26</p>
 <p>شیاد هاسرس دو فو کند لائتم و فز سجد شدات زجو فده تمتت شیاد هاسرس د وقو قبل نحات شدات و فو ایت فده تم</p>	 <p>مرکتت ستره سروفی انجیح دان ستره در فهد مرکتت ولس دان ستره در فهد مرکتت ناکب کلاعت دان رکتت در فهد ستره سروف کد ۱۴۱۸ ان ستره مرکتت</p>
<p>(e) Image 27</p>	<p>(f) Image 30</p>

Referring to Figure 6, it is apparent that the OJM images manifested variations in the locations of corruption. Each image exhibited distinct areas of corruption, highlighting the heterogeneous nature of

the corruption patterns present within the OJM dataset utilized in this research.

Figures 7, 8, 9, 10, 11 and 12 show the binary segmentation results for all comparison models for Image 4, Image 10, Image 12, Image 26, Image 27 and Image 30, respectively. It is worth noting that for the binary segmentation results, we designated the text of the OJM images as black (0 in pixels) and the background as white (1 in pixels), given that all the text within the OJM images was originally depicted in black.

Figure 7

Comparison of Binary Segmentation Results for GRS, MGRSM, and MGRSB Models on Image 4

GRS Model	MGRSM Model	MGRSB Model
بايکت دان فصسرت هئ بي هغکف تر بیتن د حاله ایتله د ر د بر جمفوی رد حوات فدان تی ۲	بايکت دان فصسرت هئ بي هغکف تر بیتن د حاله ایتله د ر د بر جمفوی رد حوات فدان تی ۲	بايکت دان فصسرت هئ بي هغکف تر بیتن د حاله ایتله د ر د بر جمفوی رد حوات فدان تی ۲
(a)	(b)	(c)

Figure 8

Comparison of Binary Segmentation Results for GRS, MGRSM, and MGRSB Models on Image 10

GRS Model	MGRSM Model	MGRSB Model
لاکي ۲ بیغ کو بیغ کولیتن برضارت اوتوما، یت دان سبایک ۲ هاری مولات برینا یولوت درود بیتیا امان مکانتق بیغ هاند	لاکي ۲ بیغ کو بیغ کولیتن برضارت اوتوما، یت دان سبایک ۲ هاری مولات برینا یولوت درود بیتیا امان مکانتق بیغ هاند	لاکي ۲ بیغ کو بیغ کولیتن برضارت اوتوما، یت دان سبایک ۲ هاری مولات برینا یولوت درود بیتیا امان مکانتق بیغ هاند
(a)	(b)	(c)

Figure 9

Comparison of Binary Segmentation Results for GRS, MGRSM, and MGRSB Models on Image 12

GRS Model	MGRSM Model	MGRSB Model
بند فروقت این بايکي بايغ ان، تکسوان فرقه درکو ان مکلا اوزن فروقت اوب بايکي سايغ ان، تکسوان وجمن بالهت شهنان هارین تلارن ایت مالک	بند فروقت این بايکي بايغ ان، تکسوان فرقه درکو ان مکلا اوزن فروقت اوب بايکي سايغ ان، تکسوان وجمن بالهت شهنان هارین تلارن ایت مالک	بند فروقت این بايکي بايغ ان، تکسوان فرقه درکو ان مکلا اوزن فروقت اوب بايکي سايغ ان، تکسوان وجمن بالهت شهنان هارین تلارن ایت مالک
(a)	(b)	(c)

Figure 10

Comparison of Binary Segmentation Results for GRS, MGRSM, and MGRSB Models on Image 26

GRS Model	MGRSM Model	MGRSB Model
(a)	(b)	(c)

Figure 11

Comparison of Binary Segmentation Results for GRS, MGRSM, and MGRSB Models on Image 27

GRS Model	MGRSM Model	MGRSB Model
(a)	(b)	(c)

Figure 12

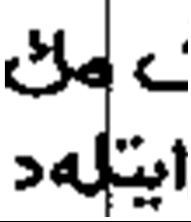
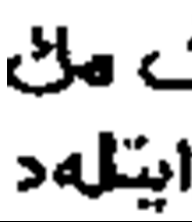
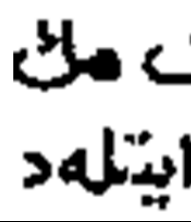
Comparison of Binary Segmentation Results for GRS, MGRSM, and MGRSB Models on Image 30

GRS Model	MGRSM Model	MGRSB Model
(a)	(b)	(c)

As demonstrated in Figures 7, 8, 9, 10, 11 and 12, the binary segmentation results achieved by the MGRSM model outperformed those of other models, effectively segmenting the text while adeptly removing corruption areas from the OJM images. As for the MGRSB model, some OJM images still retained remnants of the corruption area, resulting in the presence of residual corruption lines. While the GRS model managed to segment the text, it also segmented the corrupted region due to the absence of the inpainting technique in the GRS formulation. Figure 13 demonstrates the zoomed segmentation results of Image 4 in Figure 7 for all the comparison models.

Figure 13

Zoomed Segmentation Results of OJM Image 4 for GRS, MGRSM and MGRSB Models

GRS Model	MGRSM Model	MGRSB Model
		

As shown in Figure 13, although the MGRSB model can remove the corruption area comparably to the MGRSM model, it is also slightly removed from the text of the OJM image and the circle inside the letter ‘mim (م)’ cannot be seen. In contrast, the GRS model clearly segmented the entire text and the corruption areas as well. These observations are based on experts’ feedback.

The success of the MGRSM model can be attributed to its integration of the GRS model, renowned for segmenting intensity inhomogeneity images (Saibin & Jumaat, 2023) and the Mumford-Shah inpainting model, which is better at restoring images than the Bertalmio inpainting model (Zainal et al., 2022). The MGRSM model stands out for its ability to reconstruct images by minimizing an energy functional that achieves a balance between preserving the original image’s fidelity and ensuring smoothness within segmented regions. In contrast to the Bertalmio model, which extends linear structures into missing areas using partial differential equations (PDEs), the Mumford-Shah model excels at preserving sharp edges while seamlessly filling in gaps.

Despite the MGRSM model’s overall effectiveness in segmenting the text of the OJM images, the feedback from the experts revealed that there were certain instances where it encountered difficulties in accurately segmenting while restoring the text of the corrupted OJM images, as shown in Figures 14 and 15.

Based on Figures 14 and 15, the first column displays two real corrupted OJM images: Image 9 and Image 29, respectively. Image 9 displays a large corrupted area relative to the text size while Image 29 demonstrates a very thin line that corrupted the text. As depicted

in Figure 14(c), the MGRSM model could segment almost all the text and effectively remove the OJM image's corruption area. However, it also inadvertently removed a portion of the text where the corruption overlapped with the text. Conversely, Figure 15(c) illustrates that the MGRSM model can segment nearly all the text in the image but also segment the corruption line.

Based on the analysis and comparison of the segmentation results, as well as expert evaluations, we can conclude that the proposed MGRSM model stands out as the most optimal for restoring and segmenting the text of the real corrupted OJM images. Its effectiveness stems from its utilization of the GRS model for intensity inhomogeneity segmentation, integration of the Mumford-Shah inpainting model for image restoration, and implementation of a Gaussian function in the level set regularization process.

Figure 14

Limitation of MGRSM Model in Segmenting OJM Image 9

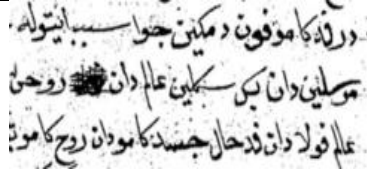
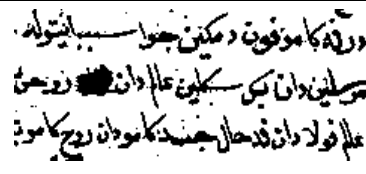
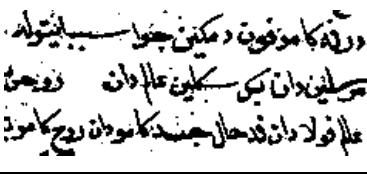
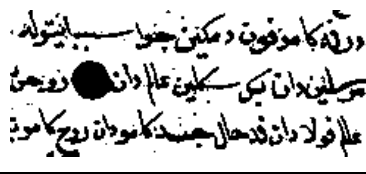
OJM Image	GRS Model
	
(a)	(b)
MGRSM Model	MGRSB Model
	
(c)	(d)

Figure 15

Limitation of MGRSM Model in Segmenting OJM Image 29

OJM Image	GRS Model
<p>من تیسکڑ بھکیں دووا انتق فرامفوات دد ماتو باکھیتا الحمال سارث صودرا دد برتند بقر اولیہ انتق فرامفوات ایش</p>	<p>من تیسکڑ بھکیں دووا انتق فرامفوات دد ماتو باکھیتا الحمال سارث صودرا دد برتند بقر اولیہ انتق فرامفوات ایش</p>
(a)	(b)
MGRSM Model	MGRSB Model
<p>من تیسکڑ بھکیں دووا انتق فرامفوات دد ماتو باکھیتا الحمال سارث صودرا دد برتند بقر اولیہ انتق فرامفوات ایش</p>	<p>من تیسکڑ بھکیں دووا انتق فرامفوات دد ماتو باکھیتا الحمال سارث صودرا دد برتند بقر اولیہ انتق فرامفوات ایش</p>
(c)	(d)

Experiment 2: Sensitivity Analysis of Parameter

Since the MGRSM model has been proven to be the most optimal for restoring and segmenting the text of the real corrupted OJM images, the parameter sensitivity of the MGRSM model will be evaluated, focusing specifically on the standard deviation parameter σ . The MGRSM model depends on the inner and outer local averages. Successfully attaining relevant and accurate segmentation results for each of the 30 OJM images depends on manually setting this parameter σ through a trial-and-error process. The parameter σ regulated the size of the inner and outer local averages within the MGRSM formulations, facilitating the local approximation of the contour's inner and outer average intensities in a Gaussian window (Azam et al., 2023). Figure 16 displays the segmentation results of the MGRSM model for Image 4, showcasing the impact of varying values of parameters σ on the segmentation outcome.

Based on Figure 16, employing too low or low parameter σ values resulted in unfavorable segmentation outcomes. Conversely, utilizing the optimal value of σ yielded better segmentation results.

Interestingly, even with high or too high parameter σ values, better segmentation outcomes were achieved. Table 3 illustrates the efficiency of the MGRSM model in segmenting the text in Image 4, considering various values of σ .

Figure 16

Segmentation Results of Image 4 with Different Parameter σ Values using MGRSM Model

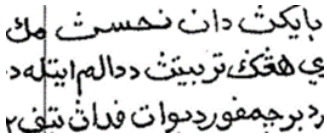
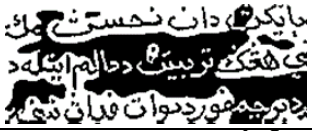
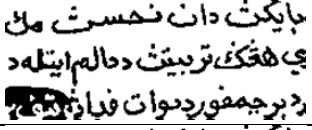
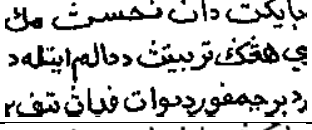
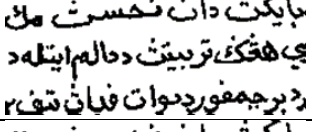
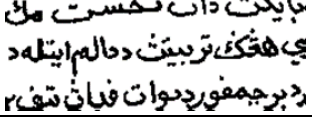
Image 4	Value of Parameter σ	Binary Segmentation Result
	Too Low: $\sigma = 1$	
	Low: $\sigma = 10$	
	Optimum: $\sigma = 20$	
	High: $\sigma = 50$	
	Too High: $\sigma = 100$	

Table 3

Overall Total Scores of Expert Evaluations and Average Elapse Time

Value of Parameter σ	Average Elapsed Time \bar{t}_i (seconds)
Too Low:	14.92
Low:	7.76
Optimum:	8.37
High:	17.70
Too High:	23.36

From the findings presented in Table 3, it can be observed that when the value of $\sigma = 10$, the average elapsed time \bar{t} was the fastest (7.76 seconds). However, its corresponding segmentation result was not as satisfactory as the optimum, high and too-high values of σ . On the other hand, the optimal value ($\sigma = 20$) required 8.37 seconds, which is the fastest compared with $\sigma = 50$ and $\sigma = 100$. Therefore, it can be concluded that selecting the optimum value of σ is crucial for obtaining better segmentation results while keeping computational costs low when using the MGRSM model. Choosing an incorrect value of σ can result in undesirable outcomes (when set too low or low) or increased computational costs (when set too high or high).

These results have significant practical implications for users of the MGRSM model. We highlight the critical importance of selecting the correct σ value to avoid poor segmentation outcomes or unnecessarily long processing times. Automating the selection of σ could streamline the process, reducing manual effort and enhancing efficiency. Additionally, the model's flexibility in handling a range of σ values suggests its adaptability to other types of images, provided the parameter is appropriately adjusted. Overall, this analysis underscores the importance of precise parameter tuning to balance segmentation

CONCLUSION

The primary objective of this study was to segment the text (foreground) of OJM images while restoring the corrupted area. To accomplish this goal, we introduced two new modified models: the MGRSM and MGRSB models. These models were developed by integrating information from the Mumford-Shah and Bertalmio inpainting models as new fitting terms into the GRS model formulation, respectively. After reformulating two proposed models, we developed MATLAB codes and implemented the algorithms on 30 real corrupted OJM images using MATLAB R2021a software. After analyzing and comparing the segmentation results as well as considering expert evaluations, we can infer that the proposed MGRSM model was the most optimal in segmenting the text of the OJM images while also restoring corrupted areas. Although the MGRSM model demonstrates commendable performance, achieving optimal results for each OJM

image involves a trial-and-error process to determine the best value of the parameter σ . Despite this need for careful tuning, the MGRSM model significantly aids in the preservation and digital restoration of valuable manuscripts, ensuring that the textual content remains accessible and legible for future generations.

In the future, we aim to extend the MGRSM model into a vector-valued (color) framework, allowing its application to color documentation images without converting to grayscale, thereby avoiding data loss. Additionally, the study did not establish a system to rank OJM documents by the severity of corruption. Implementing such a ranking system would likely require expert evaluation, which could be valuable for future studies. We also did not explore the proposed model's sensitivity to different noise types or its adaptability to various manuscript styles; areas that future research could address to enhance the proposed model's robustness. Further studies might explore alternative inpainting techniques and improve computational efficiency by implementing parallel computing.

ACKNOWLEDGMENT

This work was supported by the Pembiayaan Yuran Penerbitan Artikel (PYPA), Tabung Dana Kecemerlangan Pendidikan (DKP), Universiti Teknologi MARA (UiTM), Malaysia 2024.

REFERENCES

- Ali, H., Rada, L., & Badshah, N. (2018). Image segmentation for intensity inhomogeneity in presence of high noise. *IEEE Transactions on Image Processing*, 27(8), 3729-3738. <https://doi.org/10.1109/TIP.2018.2825101>
- Ashikhmin, M. (2001). Synthesizing natural textures. In *Proceedings of the 2001 Symposium on Interactive 3D graphics (I3D '01)* (pp. 217–226). Association for Computing Machinery. <https://doi.org/10.1145/364338.364405>
- Azam, A. S. B., Jumaat, A. K., Maasar, M. A., Laham, M. F., & Rahman, N. N. A. (2023). Local image fitting-based active contour for vector-valued images. *Indonesian Journal of Electrical Engineering and Computer Science*, 32(1), 227-235. <https://doi.org/10.11591/ijeecs.v32.i1.pp227-235>

- Badshah, N., Atta, H., Ali Shah, S. I., Attaullah, S., Minallah, N., & Ullah, M. (2020). New local region based model for the segmentation of medical images. *IEEE Access*, 8, 175035–175053. <https://doi.org/10.1109/ACCESS.2020.3017805>
- Baihaqi, Yanti, Y., & Malahayati. (2024). Ancient manuscript image enhancement method using local and global histogram equalization. *Jurnal Serambi Engineering*, 9(3), 102-10263. <https://jse.serambimekkah.id/index.php/jse/article/view/449>
- Barbu, T. (2018). Second-order anisotropic diffusion-based framework for structural inpainting. *Proceedings of the Romanian Academy, Series A: Mathematics, Physics, Technical Sciences, Information Science*, 19(2), 329-336. <https://acad.ro/sectii2002/proceedings/doc2018-2/Art03Barbu.pdf>
- Biswas, S., & Hazra, R. (2021). A level set model by regularizing local fitting energy and penalty energy term for image segmentation. *Signal Processing*, 183, 108043. <https://doi.org/10.1016/j.sigpro.2021.108043>
- Bertalmio, M. (2001). Processing of flat and non-flat image information on arbitrary manifolds using partial differential equations. University of Minnesota. https://www.maths.univ-evry.fr/pages_perso/vtorri/files/UV/unpaint/thesis-bertalmio.pdf
- Burrows, L., Patel, J., Islim, A. I., Jenkinson, M. D., Mills, S. J., & Chen, K. (2024). A semi-automatic segmentation method for meningioma developed using a variational approach model. *The Neuroradiology Journal*, 37(2), 199-205. <https://doi.org/10.1177/19714009231224442>
- Chan, T. F., & Vese, L. A. (2001). Active contours without edges. *IEEE Transactions on Image Processing*, 10(2), 266-277. <https://doi.org/10.1109/83.902291>
- Devadass, V., Bakar, J. A., Harun, N. H., & Zamri, M. F. (2021). Image enhancement system for the restoration of Old Jawi Malay manuscripts using binarization method. *Journal of Physics: Conference Series*, 1997(1), 012037. <https://doi.org/10.1088/1742-6596/1997/1/012037>
- Esedoglu, S., & Shen, J. (2002). Digital inpainting based on the Mumford–Shah–Euler image model. *European Journal of Applied Mathematics*, 13(4), 353-370. <https://doi.org/10.1017/S0956792502004904>
- Fang, J., Liu, H., Liu, J., Zhou, H., Zhang, L., & Liu, H. (2021). Fuzzy region-based active contour driven by global and local fitting energy for image segmentation. *Applied Soft Computing*, 100, 106982. <https://doi.org/10.1016/j.asoc.2020.106982>

- Gui, L., Ma, J., & Yang, X. (2023). Variational models and their combinations with deep learning in medical image segmentation: A survey. In K. Chen, C.-B. Schönlieb, X.-C. Tai, & L. Younes (Eds.), *Handbook of mathematical models and algorithms in computer vision and imaging: Mathematical imaging and vision* (pp. 1001-1022). Springer International Publishing. https://doi.org/10.1007/978-3-030-98661-2_109
- Hays, J., & Efros, A. A. (2023). Scene completion using millions of photographs. In *Seminal Graphics Papers: Pushing the Boundaries, Volume 2* (1st ed., pp. 679–685). Association for Computing Machinery. <https://doi.org/10.1145/3596711.3596783>
- Huang, J. B., Kopf, J., Ahuja, N., & Kang, S. B. (2013). Transformation guided image completion. In *IEEE International Conference on Computational Photography (ICCP)* (pp. 1-9). IEEE. <https://doi.org/10.1109/ICCPPhot.2013.6528313>
- Iqbal, E., Niaz, A., Memon, A. A., Asim, U., & Choi, K. N. (2020). Saliency-driven active contour model for image segmentation. *IEEE Access*, 8, 208978-208991. <https://doi.org/10.1109/ACCESS.2020.3038945>
- Ismail, S. M., & Abdullah, S. N. H. S. (2014). Novel binarization method for enhancing ancient and historical manuscript images. In *Human-inspired computing and its applications* (pp. 394-403). Springer. https://doi.org/10.1007/978-3-319-13647-9_36
- Jaidilert, S., & Farooque, G. (2018). Crack detection and images inpainting method for Thai mural painting images. In 2018 IEEE 3rd International Conference on Image, Vision and Computing (ICIVC) (pp. 143-148). IEEE. <https://doi.org/10.1109/ICIVC.2018.8492735>
- Kaur, A., Raj, A., Jayanthi, N., & Indu, S. (2020). Inpainting of irregular holes in a manuscript using U-Net and partial convolution. In *2020 Second International Conference on Inventive Research in Computing Applications (ICIRCA)* (pp. 526-531). IEEE. <https://doi.org/10.1109/ICIRCA48905.2020.9182917>
- Kumpulan Penyelidikan Etnomatematik Melayu. (2021). *Manuskrip Melayu*. Universiti Putra Malaysia. https://inspem.upm.edu.my/laboratori/laboratori_etnomatematik_dan_didaktik/kumpulan_penyelidikan_etnomatematik_melayu_kupelema-54857
- Mahmor, N. B., Azmi, M. S. B., & Abdullah, M. B. (2018). Image thresholding for Malay ancient manuscript (Terengganu Inscribed Stone). *International Journal of Advances in Computer Science and Technology*, 7(10). <https://doi.org/10.30534/ijacst/2018/017102018>

- Mohd Sharif, N. A., Harun, N. H., & Yusof, Y. (2024). Colour image enhancement model of retinal fundus image for diabetic retinopathy recognition. *Journal of Information and Communication Technology*, 23(2), 293-334. <https://doi.org/10.32890/jict2024.23.2.5>
- Mumford, D., & Shah, J. (1989). Optimal approximations by piecewise smooth functions and associated variational problems. *Communications on Pure and Applied Mathematics*, 42, 577-685. <https://doi.org/10.1002/cpa.3160420503>
- Othman, M., Abdullah, S. L. S., Ahmad, K. A., Bakar, M. N. A., & Mansor, A. R. (2016). The fusion of edge detection and mathematical morphology algorithm for shape boundary recognition. *Journal of Information and Communication Technology*, 15(1), 133-144. <http://e-journal.uum.edu.my/index.php/jict/article/view/8175>
- Razak, Z. (2016). *Old Jawi manuscript: Digital recognition* [Doctoral thesis, University of Malaya]. University of Malaya Students' Repository. <http://studentsrepo.um.edu.my/id/eprint/>
- Saddami, K., Munadi, K., Muchallil, S., & Arnia, F. (2017). Improved thresholding method for enhancing Jawi binarization performance. In *2017 14th IAPR International Conference on Document Analysis and Recognition (ICDAR)*. <https://doi.org/10.1109/ICDAR.2017.183>
- Saibin, T. C., & Jumaat, A. K. (2023). Variational selective segmentation model for intensity inhomogeneous image. *Indonesian Journal of Electrical Engineering and Computer Science*, 29(1), 277-285. <https://doi.org/10.11591/ijeecs.v29.i1.pp277-285>
- Schönlieb, C. B. (2015a). The Mumford-Shah image model for inpainting. In *Partial differential equation methods for image inpainting*. Cambridge University Press. <https://doi.org/10.1017/CBO9780511734304>
- Schönlieb, C. B. (2015b). Transport inpainting. In *Partial differential equation methods for image inpainting*. Cambridge University Press. <https://doi.org/10.1017/CBO9780511734304>
- Shen, J., & Chan, T. F. (2002). Mathematical models for local nontexture inpaintings. *SIAM Journal on Applied Mathematics*, 62(3), 1019-1043. <https://doi.org/10.1137/S0036139900368844>
- Som, H. M., Zain, J. M., & Ghazali, A. J. (2011). Application of threshold techniques for readability improvement of Jawi historical manuscript images. *Advanced Computing: An International Journal*, 2, 60-69. <https://doi.org/10.5121/acij.2011.2206>

- Soomro, S., Munir, A., & Choi, K. N. (2019). Fuzzy C-means clustering based active contour model driven by edge scaled region information. *Expert Systems with Applications*, 120, 387–396. <https://doi.org/10.1016/j.eswa.2018.10.052>
- Tsai, A., Yezzi, A., & Willsky, A. S. (2001). Curve evolution implementation of the Mumford-Shah functional for image segmentation, denoising, interpolation, and magnification. *IEEE Transactions on Image Processing*, 10(8), 1169-1186. <https://doi.org/10.1109/83.935033>
- Ventzas, D., Ntogas, N., & Ventza, M. M. (2012). Digital restoration by denoising and binarization of historical manuscript images. In D. Ventzas (Ed.), *Advanced image acquisition, processing techniques and applications* (pp. 73–108). InTech. <https://doi.org/10.5772/36734>
- Vese, L. A., & Chan, T. F. (2002). A multiphase level set framework for image segmentation using the Mumford and Shah model. *International Journal of Computer Vision*, 50(3), 271–293. <https://doi.org/10.1023/A:1020874308076>
- Weng, G., Dong, B., & Lei, Y. (2021). A level set method based on additive bias correction for image segmentation. *Expert Systems with Applications*, 185, 115633. <https://doi.org/10.1016/j.eswa.2021.115633>
- Yahya, S. R., Omar, K., Abdullah, S., & Sophian, A. (2018). Image enhancement background for high damage Malay manuscripts using adaptive threshold binarization. *International Journal on Advanced Science, Engineering and Information Technology*, 8(4-2), 1552-1564. <https://core.ac.uk/download/pdf/296919122.pdf>
- Yang, Y., Jia, W., & Wu, B. (2020). Simultaneous segmentation and correction model for color medical and natural images with intensity inhomogeneity. *The Visual Computer*, 36, 717-731. <https://doi.org/10.1007/s00371-019-01651-4>
- Yousef, R., Khan, S., Gupta, G., Siddiqui, T., Albahlal, B. M., Alajlan, S. A., & Haq, M. A. (2023). U-Net-based models towards optimal MR brain image segmentation. *Diagnostics*, 13(9). <https://doi.org/10.3390/diagnostics13091624>
- Yu, J., Lin, Z., Yang, J., Shen, X., Lu, X., & Huang, T. S. (2019). Free-form image inpainting with gated convolution. In *Proceedings of The IEEE/CVF International Conference on Computer Vision* (pp. 4471-4480). <https://doi.org/10.48550/arXiv.1806.03589>
- Zainal, N. N., Yuri, N. F. M., & Jumaat, A. K. (2022). Restoration of old Malay Jawi manuscripts using Mumford-Shah and

- Bertalmio inpainting models. *Malaysian Journal of Computing*, 7(1), 1047-1055. <https://myjms.mohe.gov.my/index.php/mjoc/article/view/14882>
- Zhang, L., Chen, Q., Hu, B., & Jiang, S. (2020). Text-guided neural image inpainting. In *Proceedings of the 28th ACM International Conference on Multimedia (MM '20)* (pp. 1302–1310). Association for Computing Machinery. <https://doi.org/10.1145/3394171.3414017>
- Zhao, Y., Price, B., Cohen, S., & Gurari, D. (2019). Guided image inpainting: Replacing an image region by pulling content from another image. In *2019 IEEE Winter Conference on Applications of Computer Vision (WACV)* (pp. 1514-1523). IEEE. <https://doi.org/10.1109/WACV.2019.00166>
- Zulcaffle, T.M.A., Othman, A.K., Abidin, W.A. W.Z., Mohammaddan, S., & Marzuki, A. S. W. (2010). A thresholding algorithm for text/background segmentation in degraded handwritten Jawi documents. In *2010 Second International Conference on Advances in Computing, Control, and Telecommunication Technologies* (pp. 80-84). <https://doi.org/10.1109/ACT.2010.43>